Commun. Comput. Phys.
doi: 10.4208/cicp.2018.hh80.10

Vol. **24**, No. 4, pp. 1049-1072
October 2018

Nonlocal Wave Propagation in Unbounded Multi-Scale Media

Qiang Du[1], Jiwei Zhang[2,*] and Chunxiong Zheng[3]

[1] *Department of Applied Physics and Applied Mathematics, Columbia University, New York, NY 10027, USA.*
[2] *Beijing Computational Science Research Center, Beijing 100193, China.*
[3] *Department of Mathematical Sciences, Tsinghua University, Beijing 100084, China.*

Received 25 July 2017; Accepted (in revised version) 10 December 2017

Abstract. This paper focuses on the simulation of nonlocal wave propagations in unbounded multi-scale mediums. To this end, we consider two issues: (a) the design of artificial/absorbing boundary conditions; and (b) the construction of an asymptotically compatible (AC) scheme for the nonlocal operator with general kernels. The design of ABCs facilitates us to reformulate unbounded domain problems into bounded domain problems. The construction of AC scheme facilitates us to simulate nonlocal wave propagations in multi-scale mediums. By applying the proposed ABCs and the proposed AC scheme, we investigate different wave propagation behaviors in the "local" and nonlocal mediums through numerical examples.

AMS subject classifications: 49M25, 65N22, 65N06, 65R20, 82C21, 46N40, 45A05

Key words: Asymptotically compatible, absorbing boundary method, nonlocal wave equation, nonlocal wave propagation, multi-scale mediums.

1 Introduction

Nonlocal models have attracted much attention during the last decade owing to its potentially promising applications in various disciplines of science and engineering, such as the peridynamical (PD) theory of continuum mechanics, the nonlocal theory of wave propagation, and the modeling of nonlocal diffusion process, see [4, 8, 22, 34, 39]. While most existing nonlocal models are formulated on bounded domains with volume constraints, there are indeed situations in which models in infinite domains are more reasonable, such as wave propagation in an exceedingly large sample.

*Corresponding author. *Email addresses:* qd2125@columbia.edu (Q. Du), jwzhang@csrc.ac.cn (J. Zhang), czheng@math.tsinghua.edu.cn (C. Zheng)

The PD model has been proposed for studying various processes including the dynamic fracture [7, 22]. An important feature of PD models is that it involves a horizon parameter, which characterizes the interaction range of the medium. When the horizon tends to zero, the PD models formally converge to local models, wherever the latter are well-defined. In a multi-scale medium, the horizon might vary significantly within a continuum of scales. In this situation, the PD model could potentially couple together the local and nonlocal models in different regions via heterogeneous localization [28].

In this paper, we consider the numerical computation of the following Cauchy problem of nonlocal wave equations

$$(\partial_t^2+\mathcal{L}_\gamma)q(x,t)=f(x,t),\quad x\in\mathbb{R},\quad t>0, \tag{1.1}$$

$$q(x,0)=\psi_0(x),\quad \partial_t q(x,0)=\psi_1(x),\quad x\in\mathbb{R}, \tag{1.2}$$

where $q(x,t)$ represents the displacement field, $\psi_k(x)$ (k=0,1) are the initial values, $f(x,t)$ is the body force. The linear nonlocal operator $\mathcal{L}_\gamma$ (associated with γ) is defined as

$$\mathcal{L}_\gamma q(x)=\int_{\mathbb{R}}[q(x)-q(y)]\gamma\left(y-x,\frac{y+x}{2}\right)dy, \tag{1.3}$$

where the kernel function γ is nonnegative and satisfies

$$\gamma(-\alpha,\beta)=\gamma(\alpha,\beta),\quad \forall\alpha,\beta\in\mathbb{R},\quad \text{and}\quad \gamma(\alpha,\beta)=0,\ \text{if}\ |\alpha|>\delta>0. \tag{1.4}$$

Note that the horizon δ is allowed to be variable. If γ depends on the second variable, the nonlocal medium is spatially inhomogeneous.

The goal of this paper is to develop an efficient numerical scheme to compute the solution of problem (1.1)-(1.2) confined into a local region of physical interest. We are facing two difficulties:

- The simulations are implemented in multi-scale media. This necessitates us to develop numerical schemes which should be consistent to both its local limiting model ($\delta\to 0$) and the nonlocal model itself ($\delta=\mathcal{O}(1)$);
- The definition domain is unbounded. This necessitates the design of accurate artificial/absorbing boundary conditions (ABCs) to truncate the computational domain and minimize the fictitious wave reflection from the artificial boundary.

In terms of the first difficulty, it is known that the simulations in multi-scale media need to employ asymptotic compatibility (AC) schemes, a concept developed in [26, 27] to discretize the nonlocal operator. One may also refer to review papers [5, 6]. For a multi-scale model and its numerical simulation, the AC property is a key ingredient to ensure that numerical solutions of nonlocal models converge to the correct local limiting solution, as the mesh size tends to zero and the nonlocal effect diminishes. In this paper, we allow the kernel to be heterogeneous [28] and the following diffusion coefficient

$$0<\sigma(x)=\frac{1}{2}\int_{\mathbb{R}}s^2\gamma(s,x)ds<\infty, \tag{1.5}$$

is well-defined in the whole definition domain. As $\delta \to 0$, the solution of the nonlocal wave equation (1.1) will converge to the solution of local wave equation (2.3) under the assumption (1.5) and some additional conditions [8,39]. We note that AC schemes for radial γ can be found in [9,26]. Extensions to the case involving a heterogeneous coefficient but a constant horizon can be found in [25]. Analogous ideas to those in [25,26] can be used to discretize the one-dimensional nonlocal operator with general kernels, which is presented here.

To overcome the second difficulty due to the unboundedness of the domain, we use artificial boundary method (ABM) (see [17]) and review papers [11,14,31]) to work with a truncated and bounded computational domain. For wave-like problems, these boundary conditions are usually termed as ABCs or nonreflecting boundary conditions in the literature. The ABCs have been well studied for local PDEs, see [1,2,13,15,16,18,20,29,30,33]. Different from local problems, ABCs for nonlocal problems should in general be constructed on artificial layers rather than artificial boundaries due to the nonlocal interactions. This feature presents additional complications [10,36–38]. Wildman and Gazonas [36] presented a perfectly matched layer approach for peridynamics in two dimensions. Zhang et al. [37] proposed a class of approximate ABCs for one-dimensional nonlocal heat equation by using Taylor and Padé expansions. Zheng et al. [38] achieved exact ABCs for one-dimensional nonlocal heat equation by using the spatial Laplace transform. Du et al. [10] designed accurate ABCs for two-dimensional semi-discretized wave equations by applying the similar technique of potential theory. In this paper, we use the fast recursive doubling algorithm (see the Appendix for details) to compute the ABCs for the governing equation (1.1).

To simulate nonlocal wave propagations in unbounded multi-scale media, we first introduce an AC scheme to discretize the nonlocal operator (1.3) with general kernels in the same spirit of [25]. This leads to an infinite-dimensional ODE system. To derive the ABCs, we apply the Laplace transform to transform the residual exterior problem into the Laplace domain. By solving a second-order operator difference equation, we obtain a linear mapping from artificial boundary points to ghost points. This mapping involves a complex variable $z=s^2$ due to the Laplace transform. By using the Cauchy integral theorem, we may reformulate the mapping as an integral formula, and employ the inverse Laplace transform to derive a linear mapping expressed in the time domain. This linear mapping can be taken as an ABC of generalized Dirichlet-to-Dirichlet type. The resulting second-order ODE system with a finite degree of freedoms is then integrated out with a Verlet-type time integrator.

The rest of this paper is as follows. We introduce an AC scheme for the spatially nonlocal operator in Section 2. In Section 3 we construct a fast and accurate ABC, and develop a Verlet-type temporal solver. In Section 4, three examples are reported to validate the second-order accuracy and the AC property of the proposed numerical scheme. In particular, we numerically investigate a wave propagation problem based on the nonlocal wave equation (1.1) with a continuum of scales of horizon. We compare the differ-

ent wave propagation behaviors in the nonlocal medium with $\delta=\mathcal{O}(1)$ and the "local" medium with $\delta\to 0$. We conclude this paper with a discussion in Section 5.

2 Asymptotically compatible approximation of nonlocal operator

We use this section to discuss an AC scheme. Note that the nonlocal operator $\mathcal{L}_\delta$ defined as in (1.3) is a self-adjoint operator. This is due to the fact that, for all $p,q\in C_0^\infty(\mathbb{R})$, it holds that

$$(p,\mathcal{L}_\gamma q)_{L^2(\mathbb{R})}=\frac{1}{2}\int_{\mathbb{R}}\int_{\mathbb{R}}[p(x)-p(y)][q(x)-q(y)]\gamma\left(y-x,\frac{y+x}{2}\right)dydx.$$

Given a sequence of nonlocal operators $\mathcal{L}_{\gamma_\delta}$ parameterized by a parameter $\delta>0$ with the following kernel functions

$$\gamma_\delta(\alpha,\beta)=\frac{1}{\delta^3}\gamma\left(\frac{\alpha}{\delta},\beta\right), \tag{2.1}$$

it is straightforward to verify that

$$(p,\mathcal{L}_{\gamma_\delta}q)_{L^2(\mathbb{R})}=\frac{1}{2\delta^3}\int_{\mathbb{R}}\int_{\mathbb{R}}[p(x)-p(y)][q(x)-q(y)]\gamma\left(\frac{y-x}{\delta},\frac{y+x}{2}\right)dydx.$$

Formally, we are led to

$$\lim_{\delta\to 0^+}(p,\mathcal{L}_{\gamma_\delta}q)_{L^2(\mathbb{R})}=\int_{\mathbb{R}}\sigma(x)p'(x)q'(x)dy,\quad \sigma(x)=\frac{1}{2}\int_{\mathbb{R}}s^2\gamma(s,x)ds. \tag{2.2}$$

The above arguments imply that under the scaling condition (2.1), the nonlocal operators $\mathcal{L}_{\gamma_\delta}$ converge to a local self-adjoint operator $\mathcal{L}_{\gamma_0}$ defined by

$$\mathcal{L}_{\gamma_0}q(x)=-\partial_x[\sigma(x)\partial_x q(x)]. \tag{2.3}$$

We now consider the numerical discretization of $\mathcal{L}_\gamma$. Let $\{x_n\}_{n\in\mathbb{Z}}$ be a sequence of grid points with an equidistant grid size h. For all $x\in\mathbb{R}$, we use the notation ϕ_x as the standard hat function of width h centered at point x. Let us put

$$F_q(x,y,s)=\frac{q(x)-q(y)}{y-x}s\gamma\left(s,\frac{y+x}{2}\right).$$

According to the definition (1.3), it holds that

$$\mathcal{L}_\gamma q(x)=\int_{\mathbb{R}}F_q(x,y,y-x)dy. \tag{2.4}$$

We first approximate the function $F_q(x,y,s)$ with its linear finite element interpolation with respect to the y variable, namely,

$$F_q(x,y,s)\approx\sum_{m\in Z}\phi_{x_m}(y)F_q(x,x_m,s)\equiv F_q^h(x,y,s).$$

The spatial discretization of the nonlocal operator $\mathcal{L}_\delta$ is then derived by replacing F_q in (2.4) with F_q^h:

$$\begin{aligned}
\mathcal{L}_\gamma^h q(x_n) &= \int_{\mathbb{R}} F_q^h(x_n,y,y-x_n)dy \\
&= \sum_{m\in\mathbb{Z}} \int_{\mathbb{R}} \phi_{x_m}(y) F_q(x_n,x_m,y-x_n)dy \\
&= \sum_{m\in\mathbb{Z}} \int_{\mathbb{R}} \phi_{x_m}(y) \frac{q(x_n)-q(x_m)}{(m-n)h}(y-x_n)\gamma\left(y-x_n,\frac{x_n+x_m}{2}\right)dy \\
&= \sum_{m\in\mathbb{Z}} \int_{\mathbb{R}} \phi_{(m-n)h}(s) \frac{q(x_n)-q(x_m)}{(m-n)h} s\gamma\left(s,\frac{x_n+x_m}{2}\right)ds \\
&= \sum_{m\in\mathbb{Z},m\neq n} \int_{\mathbb{R}} \phi_{(m-n)h}(s) \frac{q(x_n)-q(x_m)}{(m-n)h} s\gamma\left(s,\frac{x_n+x_m}{2}\right)ds \\
&= \sum_{m\in\mathbb{Z}} a_{n,m} q(x_m), \qquad (2.5)
\end{aligned}$$

where we have put

$$a_{n,m} = \begin{cases} -\dfrac{1}{(n-m)h}\displaystyle\int_{\mathbb{R}} \phi_{(n-m)h}(s) s\gamma\left(s,\frac{x_n+x_m}{2}\right)ds, & m\neq n, \\ -\displaystyle\sum_{m\neq n} a_{n,m}, & m=n. \end{cases}$$

It is straightforward to verify that

$$a_{n,m} = a_{m,n}, \quad n,m\in\mathbb{Z}.$$

This implies that the discrete nonlocal operator $\mathcal{L}_\gamma^h$ is symmetric.

The above discretization is also asymptotically compatible. This can be verified when the kernel function γ is compactly supported over a strip $[-\delta_0,\delta_0]\times\mathbb{R}$. In this case, if $\delta\leq h/\delta_0$, a direct computation shows that

$$\begin{aligned}
&\mathcal{L}_{\gamma_\delta}^h q(x_n) = \sum_{m=n\pm1} \int_{\mathbb{R}} \phi_{(m-n)h}(s) \frac{q(x_n)-q(x_m)}{(m-n)h\delta^3} s\gamma\left(\frac{s}{\delta},\frac{x_n+x_m}{2}\right)ds \\
=&\frac{q(x_n)-q(x_{n+1})}{h^2\delta^3}\int_0^h s^2\gamma\left(\frac{s}{\delta},x_{n+\frac{1}{2}}\right)ds - \frac{q(x_{n-1})-q(x_n)}{h^2\delta^3}\int_0^h s^2\gamma\left(\frac{s}{\delta},x_{n-\frac{1}{2}}\right)ds \\
=&\frac{\sigma_{n+\frac{1}{2}}(q(x_n)-q(x_{n+1}))}{h^2} - \frac{\sigma_{n-\frac{1}{2}}(q(x_{n-1})-q(x_n))}{h^2},
\end{aligned}$$

where we have set

$$\sigma_{n+\frac{1}{2}} = \sigma(x_{n+\frac{1}{2}}), \quad n\in\mathbb{Z}.$$

This implies that the discrete nonlocal operator $\mathcal{L}^h_{\gamma_\delta}$ reduces to a second-order centered difference approximation for the limiting local diffusion operator $\mathcal{L}_{\gamma_0}$. We remark that the above analysis of AC property works only for the nearest neighbor case, one can see the proof in [26] for cases with multiple interaction neighbors as well. Additional discussions in the multidimensional space can be found in [9].

We now consider how to model the kernel function $\gamma(\alpha,\beta)$ by taking $\alpha=x-y$ and $\beta=\frac{x+y}{2}$. The first parameter α measures the distance between two location points, while the second parameter β relates to a reference point. Let $H=H(\alpha)$ be a reference interaction function satisfying

$$H(-\alpha)=H(\alpha),\quad \frac{1}{2}\int_{\mathbb{R}}\alpha^2 H(\alpha)d\alpha=1.$$

We can then set the kernel function as

$$\gamma(\alpha,\beta)=\frac{\sigma(\beta)}{\zeta^3(\beta)}H\left(\frac{\alpha}{\zeta(\beta)}\right), \tag{2.6}$$

where $\zeta(\beta)$ measures the local horizon and $\sigma(\beta)$ is actually the limiting diffusion coefficient function.

To compute $a_{n,m}$ with $m\neq n$, let us set

$$k=|n-m|,\quad \zeta=\zeta\left(\frac{x_n+x_m}{2}\right),\quad \sigma=\sigma\left(\frac{x_n+x_m}{2}\right).$$

A direct computation shows that

$$\begin{aligned}a_{n,m}&=-\frac{1}{kh}\int_{\mathbb{R}}\phi_{kh}(s)s\gamma\left(s,\frac{x_n+x_m}{2}\right)ds\\&=-\frac{1}{kh}\int_{\mathbb{R}}\phi_{kh}(s)s\frac{\sigma}{\zeta^3}H\left(\frac{s}{\zeta}\right)ds\\&=-\frac{\sigma}{kh\zeta}\int_{\mathbb{R}}\phi_{kh}(\zeta s)sH(s)ds.\end{aligned}$$

Note that

$$\int_{\mathbb{R}}\phi_{kh}(\zeta s)sH(s)ds=\int_{(k-1)h/\zeta}^{kh/\zeta}\frac{\zeta s-(k-1)h}{h}sH(s)ds+\int_{kh/\zeta}^{(k+1)h/\zeta}\frac{(k+1)h-\zeta s}{h}sH(s)ds.$$

The simplest constant type kernel is taken for example as:

$$H(\alpha)=\chi_{[-1,1]}(\alpha).$$

Thus, the coefficients $a_{n,m}$ $(n\neq m)$ are calculated as

$$a_{n,m}=-\frac{h\sigma\left(\frac{x_n+x_m}{2}\right)}{\zeta^3\left(\frac{x_n+x_m}{2}\right)},$$

which reflect the variable horizon and diffusion. We refer to more discussions on AC schemes in [9,25,26].

3 Absorbing boundary conditions for discrete nonlocal wave problems

When one wants to simulate the dynamical equation (1.1), the full-space problem is often truncated by constructing suitable ABCs so that the solution at the boundary is not perturbed. This requires us to reformulate the problem on unbounded domain as an initial boundary-value problem by introducing suitable boundary conditions.

To obtain ABCs, we make some additional assumptions on the initial data functions and the kernel function of the problem (1.1)-(1.2):

A1: $\psi_k(k=0,1)$ and f are compactly supported into a finite interval $[x_l,x_r]$;

A2: γ is compactly supported into a strip $[-\delta,\delta]\times\mathbb{R}$ with $\delta\leq x_r-x_l$;

A3: γ is homogeneous in both $[x_r,+\infty)$ and $(-\infty,x_l]$, namely,

$$\begin{aligned}&\gamma(\alpha,\beta)=\gamma_L(\alpha), \quad \beta\in(-\infty,x_l+\delta/2],\\ &\gamma(\alpha,\beta)=\gamma_R(\alpha), \quad \beta\in[x_r-\delta/2,+\infty).\end{aligned}$$

The functions γ_L and γ_R can be distinct. However, without loss of generality, in the sequel we assume $\gamma_L=\gamma_R=\gamma_\infty$.

Let $h=(x_r-x_l)/M$ be the spatial step size, and $x_n=x_l+nh$ be the grid points. We now introduce $N_s=0$, $N_e=M$, and

$$c_k=\begin{cases}-\dfrac{1}{kh}\displaystyle\int_{\mathbb{R}}\phi_{kh}(s)s\gamma_\infty(s)ds, & k\neq 0,\\ -\sum_{m\neq 0}c_m, & k=0.\end{cases}$$

Note that $c_{-k}=c_k$, and for all k with $|k|>L=[\delta/h]+1$, it holds that $c_k=0$. We have to point out that, for the situation of the homogeneous kernel above, the discrete scheme (2.5) reduces to the quadrature-based finite difference discretization of the formula (3.6) developed in [26].

Now applying the spatial discretization scheme developed in the last section, we derive a semi-discrete nonlocal wave problem as follows:

$$\ddot{q}_n+\sum_{m\in\mathbb{Z}}a_{n,m}q_m=f_n(t), \quad t>0, \tag{3.1}$$

$$q_n(0)=\psi_0(x_n), \quad \dot{q}_n(0)=\psi_1(x_n), \tag{3.2}$$

where $q_n(t)\approx q(x_n,t)$ and $f_n(t)=f(x_n,t)$. Due to the assumptions A1-A3, it holds that

$$\begin{aligned}&f_n=0,\ \psi_0(x_n)=0, \quad \psi_1(x_n)=0, \quad n<N_s \text{ or } n>N_e,\\ &a_{n,m}=c_{n-m}, \quad n>N_e \text{ or } n<N_s, \ m\in\mathbb{Z}.\end{aligned}$$

We can decompose the semi-discrete nonlocal problem (3.1)-(3.2) into the following three subproblems:

- Interior inhomogeneous subproblem:

$$\ddot{q}_n+\sum_{m\in\mathbb{Z}}a_{n,m}q_m=f_n(t),\quad N_s\le n\le N_e,\quad t>0, \tag{3.3}$$

$$q_n(0)=\psi_{0,n},\quad \dot{q}_n(0)=\psi_{1,n},\quad N_s\le n\le N_e; \tag{3.4}$$

- Left homogeneous subproblem:

$$\ddot{q}_n+\sum_{|m|\le L}c_m q_{n+m}=0,\quad n<N_s,\quad t>0, \tag{3.5}$$

$$q_n(0)=0,\quad \dot{q}_n(0)=0,\quad n<N_s; \tag{3.6}$$

- Right homogeneous subproblem:

$$\ddot{q}_n+\sum_{|m|\le L}c_m q_{n+m}=0,\quad n>N_e,\quad t>0, \tag{3.7}$$

$$q_n(0)=0,\quad \dot{q}_n(0)=0,\quad n>N_e. \tag{3.8}$$

None of these three subproblems are complete. However, we can manage to express $\{q_{N_s-l}\}_{l=1}^{L}$ with $\{q_{N_s+l}\}_{l=0}^{L-1}$ through the left homogeneous subproblem (3.5)-(3.6), and express $\{q_{N_e+l}\}_{l=1}^{L}$ with $\{q_{N_e-l}\}_{l=0}^{L-1}$ through the right homogeneous subproblem (3.7)-(3.8). By taking these relations as ABCs of generalized Dirichlet-to-Dirichlet (DtD) type, the interior inhomogeneous subproblem (3.3)-(3.4) becomes complete.

3.1 Reduced semi-infinite discrete nonlocal problem

Let us consider the following reduced semi-infinite discrete nonlocal problem

$$zu_n+\sum_{|m|\le L}c_m u_{n+m}=0,\quad n>0, \tag{3.9}$$

$$u_n\to 0,\quad n\to+\infty, \tag{3.10}$$

where $z\in\mathbb{C}$ is a complex parameter. We introduce the following sequence space with a bounded l^2-norm:

$$\mathfrak{l}=\Big\{u=\{u_n\}_{n\in\mathbb{Z}}:\|u\|^2=\sum_{n\in\mathbb{Z}}|u_n|^2<+\infty\Big\},$$

and its dense linear subspace

$$\mathfrak{l}_0=\{u=\{u_n\}_{n\in\mathbb{Z}}:\sharp u<+\infty\}.$$

In the above, the symbol $\sharp$ stands for the number of nonzero elements. We define the linear operator $\mathcal{T}$ acting on $\mathfrak{l}_0$ as

$$\mathcal{T}u=\left\{\sum_{|m|\le L}c_m u_{n+m}\right\}_{n\in\mathbb{Z}},\qquad u=\{u_n\}_{n\in\mathbb{Z}}.$$

Obviously, the operator $\mathcal{T}$ is symmetric and nonnegative. Let us denote by the same notation $\mathcal{T}$ as its l^2-extension to the sequence space $\mathfrak{l}$. Therefore, the spectra of $\mathcal{T}$, denoted by $\sigma(\mathcal{T})$, form a subset of $\mathbb{R}$ that lies on the right half real axis. Moreover, the spectrum radius $\rho(\mathcal{T})$ is bounded by $\sum_{|m|\leq L}|c_m|$.

Let us set

$$U_n=[u_{(n-1)L+1},\cdots,u_{nL}]^\dagger,\quad n\geq 0,$$

then the semi-infinite discrete nonlocal problem (3.9)-(3.10) can be rewritten into an equivalent second-order matrix difference equation

$$zU_n+AU_{n-1}+BU_n+A^\dagger U_{n+1}=0,\quad n\geq 1, \tag{3.11}$$

$$U_n\to 0,\quad n\to+\infty. \tag{3.12}$$

where

$$A=\begin{pmatrix} c_L & \cdots & \cdots & c_2 & c_1\\ & c_L & \cdots & \cdots & c_2\\ & & c_L & \cdots & \cdots\\ & & & \cdots & \cdots\\ & & & & c_L\end{pmatrix},\quad B=\begin{pmatrix} c_0 & c_1 & \cdots & \cdots & c_{L-1}\\ c_1 & c_0 & c_1 & \cdots & \cdots\\ \cdots & c_1 & c_0 & c_1 & \cdots\\ \cdots & \cdots & \cdots & \cdots & \cdots\\ c_{L-1} & \cdots & \cdots & c_1 & c_0\end{pmatrix}.$$

We can rewrite Eq. (3.11) as

$$U_n=A_0U_{n-1}+B_0U_{n+1},\quad n\geq 1; \tag{3.13}$$

where

$$A_0=-(z+B)^{-1}A\quad\text{and}\quad B_0=-(z+B)^{-1}A^\dagger.$$

Prescribed U_0, for all $z\notin\sigma(-\mathcal{T})$, the matrix difference system (3.12)-(3.13) admits a unique solution. By using the fast algorithm developed in the Appendix, the value of U_1 is uniquely determined by the value of U_0 in a linear manner. Therefore, there exists a linear transformation $\mathcal{K}=\mathcal{K}(z)$ (see the derivative in (A.6)), which maps U_0 to U_1 as

$$U_1=\mathcal{K}(z)U_0.$$

We remark that it is generally hard to express the matrix-valued function $\mathcal{K}(z)$ in a closed form, but this operator can be efficiently computed for any prescribed $z\notin\sigma(-\mathcal{T})$.

The operator-valued function $\mathcal{K}(z)$ is analytic in the complement of $\sigma(-\mathcal{T})$, and the infinity point is actually a zero point. Given a smooth domain Ω such that $s^2(\partial\Omega)$ encloses the spectrum $\sigma(-\mathcal{T})$ and $s^2(\Omega)\cap\sigma(-\mathcal{T})=\emptyset$, by applying the Cauchy integral formula we derive

$$\mathcal{K}(s^2)=\oint_{\partial\Omega}\frac{\mathcal{K}(\xi^2)}{s-\xi}\frac{d\xi}{2\pi i},\qquad s\in\mathbb{C}\backslash\bar{\Omega}.$$

Let

$$\int_{\partial\Omega}g(\xi)\frac{d\xi}{2\pi i}\sim\sum_{\alpha=1}^{\kappa}\omega_\alpha g(\xi_\alpha)$$

be a suitably designed numerical quadrature scheme (such as trapezoidal or midpoint rules in [35]) for the contour integral, where $\{\xi_\alpha\}_{\alpha=1}^{\kappa}$ is the set of sampling points and $\{\omega_\alpha\}_{\alpha=1}^{\kappa}$ is the set of associated quadrature weights. We derive the following rational approximation for the matrix-valued function $\mathcal{K}(s^2)$ restricted to the domain $\mathbb{C}\backslash\bar{\Omega}$:

$$\tilde{\mathcal{K}}(s^2)=\sum_{\alpha=1}^{\kappa}\frac{\omega_\alpha\mathcal{K}(\xi_\alpha^2)}{s-\xi_\alpha},\quad s\in\mathbb{C}\backslash\bar{\Omega}.$$

Note that we need only to compute a finite number of values $\mathcal{K}(\xi_\alpha^2)$ to form the above approximation, and this treatment can be performed in advance of the computation.

3.2 Truncated discrete nonlocal wave problem

Now performing the Laplace transform on the right homogeneous subproblem (3.7)-(3.8), we have

$$s^2\hat{q}_n+\sum_{|m|\le L}c_m\hat{q}_{n+m}=0,\quad n>N_e, \tag{3.14}$$

$$\hat{q}_n\to 0,\quad n\to+\infty. \tag{3.15}$$

This is a special instance of the semi-infinite discrete nonlocal problem (3.9)-(3.10) with

$$z(s)=s^2,\quad u_n=\hat{q}_{n+N_e}.$$

Choosing the domain Ω appropriately and applying the result in the last subsection, we derive an approximate DtD map in the Laplace domain as

$$[\hat{q}_{N_e+1},\cdots,\hat{q}_{N_e+L}]^\dagger=\sum_{\alpha=1}^{\kappa}\frac{\omega_\alpha\mathcal{K}(\xi_\alpha^2)}{s-\xi_\alpha}[\hat{q}_{N_e-L+1},\cdots,\hat{q}_{N_e}]^\dagger.$$

Performing the inverse Laplace transform yields

$$[q_{N_e+1},\cdots,q_{N_e+L}]^\dagger=\sum_{\alpha=1}^{\kappa}\omega_\alpha\mathcal{K}(\xi_\alpha^2)e^{\xi_\alpha t}*[q_{N_e-L+1},\cdots,q_{N_e}]^\dagger. \tag{3.16}$$

Making the analogous treatment for the left subproblem (3.5)-(3.6), we derive

$$[q_{N_s-1},\cdots,q_{N_s-L}]^\dagger=\sum_{\alpha=1}^{\kappa}\omega_\alpha\mathcal{K}(\xi_\alpha^2)e^{\xi_\alpha t}*[q_{N_s+L-1},\cdots,q_{N_s}]^\dagger. \tag{3.17}$$

The formulas (3.16) and (3.17) express the values of q_n in the *ghost region*

$$\mathcal{I}_g=[N_s-L,N_s-1]\cup[N_e+1,N_e+L]$$

via the values of q_n in the *absorbing region*

$$\mathcal{I}_a=[N_s,N_s+L-1]\cup[N_e-L+1,N_e].$$

The relations (3.16) and (3.17) can be taken as ABCs of generalized DtD type for the interior inhomogeneous subproblem (3.3)-(3.4). Applying ABCs (3.16) and (3.17), we then derive the following truncated nonlocal wave problem in the *interior region* $\mathcal{I}_i=[N_s,N_e]$:

$$\ddot{q}_n+\sum a_{n,m}q_m=f_n(t),\quad N_s\le n\le N_e,\quad t>0, \tag{3.18}$$

$$[q_{N_s-1},\cdots,q_{N_s-L}]^\dagger=\sum_{\alpha=1}^{\kappa}\omega_\alpha\mathcal{K}(\xi_\alpha^2)e^{\xi_\alpha t}*[q_{N_s-L+1},\cdots,q_{N_s}]^\dagger, \tag{3.19}$$

$$[q_{N_e+1},\cdots,q_{N_e+L}]^\dagger=\sum_{\alpha=1}^{\kappa}\omega_\alpha\mathcal{K}(\xi_\alpha^2)e^{\xi_\alpha t}*[q_{N_e+L-1},\cdots,q_{N_e}]^\dagger, \tag{3.20}$$

$$q_n(0)=\psi_{0,n},\quad \dot{q}_n(0)=\psi_{1,n},\quad N_s\le n\le N_e. \tag{3.21}$$

In the next subsection, we intend to design a Verlet-type solver for the above ODE system.

3.3 Verlet-type ODE solver

Let us denote

$$\mathcal{K}_\alpha=\omega_\alpha\mathcal{K}(\xi_\alpha^2),\quad p_{n,\alpha}(t)=e^{\xi_\alpha t}*q_n(t),\quad n\in\mathcal{I}_a,\quad \alpha\in[1,\kappa].$$

Note that the functions $p_{n,\alpha}$ satisfy the following ODE

$$\dot{p}_{n,\alpha}=\xi_\alpha p_{n,\alpha}+q_n \tag{3.22}$$

with the initial condition $p_{n,\alpha}(0)=0$.

Let us indicate $t_j=j\tau$ as the j-th time point where τ is the temporal stepsize, and introduce a new variable $v_n(t)=\partial_t q_n(t)$. We use the following notations to approximate the relevant functions:

$$q_n^j\approx q_n(t_j),\quad p_{\alpha,n}^j\approx p_{\alpha,n}(t_j),\quad v_n^{j+1/2}\approx v_n(t_{j+1/2}),\quad j\ge 0.$$

The initial values are set as

$$\begin{aligned}
&q_n^0=\psi_{0,n},\quad n\in\mathcal{I}_i\cup\mathcal{I}_g,\\
&p_{n,\alpha}^0=0,\quad n\in\mathcal{I}_a,\quad \alpha\in[1,\kappa],\\
&v_n^{1/2}=\psi_{1,n}+\frac{\tau}{2}\left[f_n(0)-\sum a_{n,m}q_m^0\right],\quad n\in\mathcal{I}_i.
\end{aligned}$$

For all $j\ge 0$, to derive q_n^{j+1}, we first apply the following second order central difference quotient approximation for the interior nodes:

$$\frac{q_n^{j+1}-q_n^j}{\tau}=v_n^{j+1/2},\quad n\in\mathcal{I}_i. \tag{3.23}$$

It is known that the exact solution of (3.22) expresses as

$$p_{n,\alpha}^{j+1}=e^{\xi_\alpha\tau}p_{n,\alpha}^{j}+\int_0^\tau e^{\xi_\alpha(\tau-s)}q_n(t_n+s)ds.$$

Using the mid-point approximation for $q_n(t_n+s)$ at $s=\tau/2$, we derive

$$p_{n,\alpha}^{j+1}=e^{\xi_\alpha\tau}p_{n,\alpha}^{j}+\frac{e^{\xi_\alpha\tau}-1}{\xi_\alpha}\left[q_n^{j+1}-\frac{\tau}{2}v_n^{j+1/2}\right],\quad n\in\mathcal{I}_a,\quad \alpha\in[1,\kappa]. \tag{3.24}$$

We then use the algebraic relations (3.19)-(3.20) to compute the values of q_n^{j+1} in the ghost region:

$$[q_{N_s-1}^{j+1},\cdots,q_{N_s-L}^{j+1}]^\dagger=\sum_{\alpha=1}^{\kappa}\mathcal{K}_\alpha[p_{N_s+L-1,\alpha}^{j+1},\cdots,p_{N_s,\alpha}^{j+1}]^\dagger, \tag{3.25}$$

$$[q_{N_e+1}^{j+1},\cdots,q_{N_e+L}^{j+1}]^\dagger=\sum_{\alpha=1}^{\kappa}\mathcal{K}_\alpha[p_{N_e-L+1,\alpha}^{j+1},\cdots,p_{N_e,\alpha}^{j+1}]^\dagger. \tag{3.26}$$

To derive $v_n^{j+3/2}$, we use the following second order central difference quotient approximation for the interior nodes:

$$\frac{v_n^{j+3/2}-v_n^{j+1/2}}{\tau}=f_n(t_{j+1})-\sum a_{n,m}q_m^{j+1},\quad n\in\mathcal{I}_i. \tag{3.27}$$

Denote T the length of the time interval, and $J=T/\tau$ the number of time step. The complexity of evaluating the Verlet-type algorithm (3.23)-(3.27) at each time-step is $\mathcal{O}((N_e-N_s+2\kappa)L)$ operations. The total computational cost for the Verlet-type algorithm is thus $\mathcal{O}(J(N_e-N_s+2\kappa)L)$ and the memory requirement is $\mathcal{O}(N_e-N_s+2\kappa L)$ for storing the solutions.

4 Numerical tests

The section above leaves two important issues which are worthy of further consideration. The first one is how to select an appropriate contour $\partial\Omega$. This issue is related to the stability of the truncated finite domain problem equipped with the approximate ABCs. The second one is how to approximate the contour integral by applying suitable quadrature scheme. This issue is related to the accuracy of the truncated problem. It turns out that both issues are problem-dependent.

In all numerical tests, we use the following Talbot contour

$$(-\pi,\pi)\to\Gamma\qquad\theta\to\xi(\theta)=\mu\theta\cot\theta+\frac{2i\nu\theta}{\pi}$$

in the s-complex plane [21, 24]. Let T be the terminal time. Considering the spectrum $\sigma(-\mathcal{L})$ lies in the negative real axis and bounded by $\sum_{|m|\le L}|c_m|$, to ensure the stability, we set

$$\mu=\frac{1}{T},\quad \nu=\sqrt{2\sum_{|m|\le L}|c_m|}.$$

Given an even integer $\kappa>0$, the quadrature points and weights are then set as

$$\theta_\alpha=-\pi+\frac{2\pi\alpha}{\kappa+1},\quad \xi_\alpha=\xi(\theta_\alpha),\quad \omega_\alpha=\frac{\xi'(\theta_\alpha)}{i(\kappa+1)},\quad \alpha\in[1,\kappa].$$

One may also refer to discussions in [35] on Talbot's method for the numerical inversion of the Laplace Transform that consists of numerically integrating the Bromwich integral on a special contour by means of the trapezoidal or midpoint rules. Furthermore, the issues on how to choose the parameters that define the contour and the geometric convergence rate are discussed.

For a typical kernel (2.6), for simplicity we always set the reference interaction function as a Gaussian function of the form

$$H(\alpha)=4\sqrt{\frac{10^3}{\pi}}e^{-10\alpha^2}.$$

Three numerical examples will be reported. We use the first two numerical examples to investigate the effectiveness of our approach from two perspectives: **(a)** the convergence of numerical scheme to the governing nonlocal equation by refining h for any fixed δ; **(b)** the asymptotic compatibility of numerical scheme by refining δ and h simultaneously, but keeping their ratio fixed. We use the third example to demonstrate the performance of our numerical approach in multi-scale media. In this situation, the governing equation contains a continuum of scales which include both the nonlocal and the asymptotically local media.

Example 4.1. We use this example to offer results of numerical simulations on the convergence of the discrete schemes (3.23)–(3.27) with the functions of local horizon and limiting diffusion coefficient given as

$$\zeta(\beta)=\delta,\quad \sigma(\beta)=1.$$

The initial values are set as

$$q(x,0)=e^{-25(x-0.2)^2}+e^{-25(x+0.2)^2}, \tag{4.1a}$$

$$q_t(x,0)=50xe^{-25x^2}. \tag{4.1b}$$

In the numerical implementation, we set the computational domain as $[-2,2]$. Fig. 1 illustrates the numerical solutions up to $T=4$ by setting $\delta=0.5$, 0.2, 0.1, 0.05, $h=2^{-8}$, $\tau=10^{-3}$, and $\kappa=200$, 400, 800, 2000, respectively.

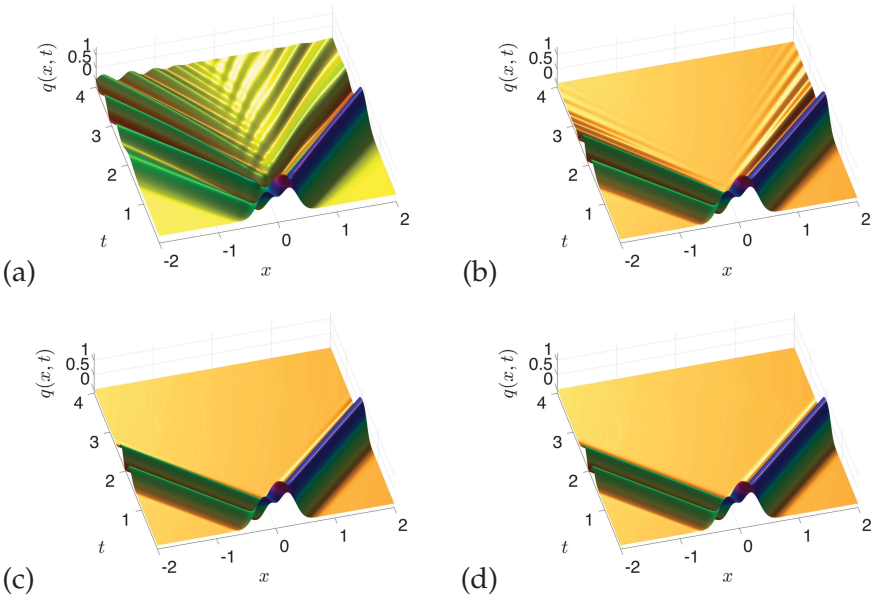

Figure 1: Wave propagation for Example 4.1. The initial values are set as in (4.1). (a): $\delta=0.5$. (b): $\delta=0.2$. (c): $\delta=0.1$. (d): $\delta=0.05$.

To investigate the quantitative accuracy of discrete scheme (3.23)-(3.27), we show in Table 1 the L^2-errors between the numerical solutions and the reference solutions, and the spatial convergence order for various horizons $\delta=0.5,0.2,0.1$. The reference solutions are obtained by the pseudo-spectral method on a sufficiently large truncated definition domain. A second order convergence rate can be observed.

Table 1: L^2-errors and convergence orders at $t=2$ for Example 4.1.

$h\backslash\delta$	$\delta=0.5$	order	$\delta=0.2$	order	$\delta=0.1$	order
2^{-3}	1.28×10^{-1}	– –	1.94×10^{-1}	– –	2.25×10^{-1}	– –
2^{-4}	3.34×10^{-2}	1.93	4.40×10^{-2}	2.14	5.38×10^{-2}	2.06
2^{-5}	8.42×10^{-3}	1.99	1.09×10^{-2}	2.01	9.73×10^{-3}	2.46
2^{-6}	2.10×10^{-3}	2.00	2.71×10^{-3}	2.01	2.39×10^{-3}	2.02
2^{-7}	5.24×10^{-4}	2.01	6.71×10^{-4}	2.01	5.91×10^{-4}	2.02

As mentioned earlier, the nonlocal operator (1.3) converges to the corresponding local operator (2.3) in the distributional sense as $\delta\to0$, see also the details in [8]. In the following, we need to verify whether our numerical discrete scheme (2.5) admits the asymptotic compatibility property. Namely, we need to check whether the numerical solutions of discrete systems (3.23)-(3.27) converge to the correct solutions of the following

local wave equation

$$\partial_t^2 q = \partial_x(\sigma(x)\partial_x q) + f(x,t), \quad x \in \mathbb{R}, \quad t > 0. \tag{4.2}$$

To achieve this, we maintain the ratio $\delta/h = \mathcal{O}(1)$ and consider the so-called "δ-convergence" of our numerical scheme [3, 23]. In Table 2, we list the L^2-errors between numerical solutions and exact solutions of the limiting local wave equation. A second-order convergence rate can be observed, which validates the asymptotic compatibility property.

Table 2: L^2-errors and δ-convergence orders between the numerical solutions of discrete scheme (3.23)-(3.27) and exact solutions of local problem (4.2) by vanishing δ and h simultaneously at $t=2$.

$h\backslash\delta$	$\delta=h$	order	$\delta=2h$	order	$\delta=3h$	order
2^{-4}	4.91×10^{-2}	– –	5.66×10^{-2}	– –	8.57×10^{-2}	– –
2^{-5}	1.25×10^{-2}	1.98	1.43×10^{-2}	1.91	2.28×10^{-2}	1.91
2^{-6}	3.12×10^{-3}	2.00	3.59×10^{-3}	1.99	5.76×10^{-3}	1.99
2^{-7}	7.80×10^{-4}	2.00	8.98×10^{-4}	2.00	1.44×10^{-3}	2.00
2^{-8}	1.94×10^{-4}	2.01	2.24×10^{-4}	2.00	3.60×10^{-4}	2.00
2^{-9}	4.80×10^{-5}	2.03	5.54×10^{-5}	2.01	8.95×10^{-5}	2.01

Example 4.2. Different from Example 4.1, we consider a spatially inhomogeneous kernel (2.6) with the following parameter functions (see Fig. 2)

$$\zeta(\beta) = \delta \times [1 + \mathrm{erfc}(\beta)], \quad \sigma(\beta) = 1 + e^{-3\beta^2}. \tag{4.3}$$

Note that the limiting local wave equation is also spatially inhomogeneous. The initial values are the same as those in Example 4.1. We set the computational domain as $[-2,2]$. Fig. 3 illustrates the evolution of numerical solutions up to $T=4$ by taking $\delta=0.5$, 0.2, 0.1, 0.05, $h=2^{-8}$, and $\kappa=50$, 100, 200, 1000, respectively.

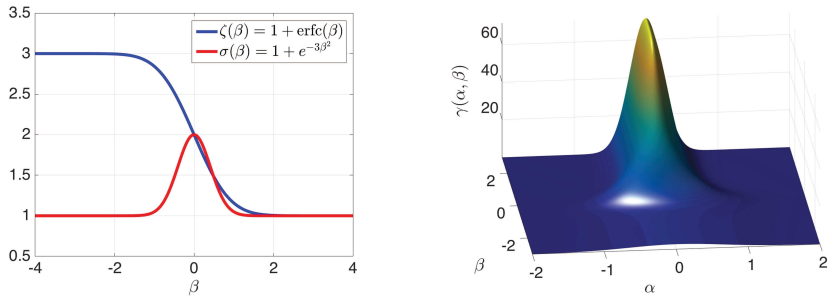

Figure 2: Kernel setting for Example 4.2. Left: plots of $\zeta(\beta)$ with $\delta=1$ and $\sigma(\beta)$. Right: associated kernel function $\gamma(\alpha,\beta)$ with $\delta=1$.

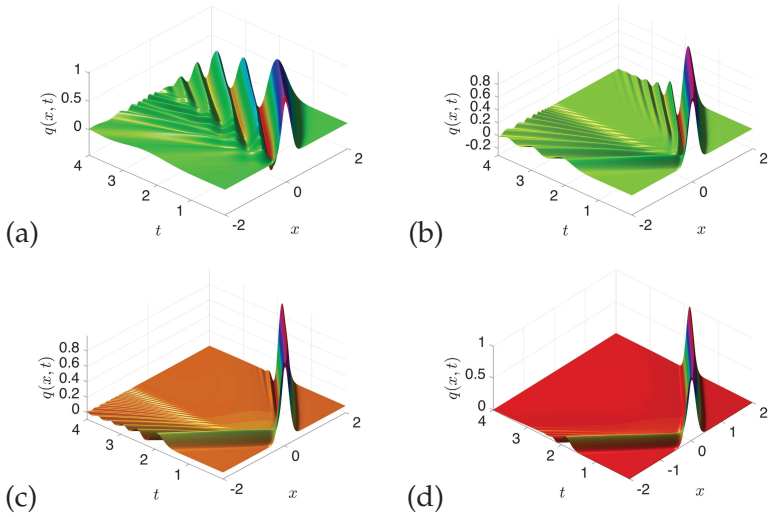

Figure 3: Wave propagation for Example 4.2. The initial values are set as in (4.1). (a): $\delta=0.5$. (b): $\delta=0.2$. (c): $\delta=0.1$. (d): $\delta=0.05$.

Table 3 shows the L^2-errors and the spatial convergence order for numerical solutions of discrete scheme (3.23)-(3.27) by refining h for given $\delta=0.5,0.2,0.1$ and $\tau=10^{-3}$. The numerical evidences verify the second order accuracy of the interior spatial discretization. In Table 4, we list the L^2-errors and δ-convergence orders between numerical solutions of the discrete scheme (3.23)-(3.27) with initial values (4.1) and the exact solution of local problem given in (4.2). Analogous to Example 4.1, a second order convergence order is

Table 3: (Example 4.2) L^2-errors and convergence orders by reducing h for $\delta=1$, 0.5, 0.2 at $t=2$.

$h\backslash\delta$	$\delta=1$	order	$\delta=0.5$	order	$\delta=0.2$	order
2^{-3}	1.98×10^{-2}	– –	6.28×10^{-2}	– –	1.88×10^{-1}	– –
2^{-4}	4.97×10^{-3}	2.00	1.58×10^{-2}	1.99	4.27×10^{-2}	2.15
2^{-5}	1.24×10^{-3}	2.00	3.94×10^{-3}	2.00	1.07×10^{-2}	2.00
2^{-6}	3.11×10^{-4}	2.00	9.84×10^{-4}	2.00	2.66×10^{-3}	2.01

Table 4: (Example 4.2) L^2-errors and δ-convergence of numerical solutions of discrete scheme (3.23)-(3.27) to exact solutions of local problem (4.2) at $t=1$.

$h\backslash\delta$	$\delta=h/2$	order	$\delta=h$	order	$\delta=2h$	order
2^{-5}	1.81×10^{-2}	–	1.88×10^{-2}	–	3.20×10^{-2}	–
2^{-6}	4.53×10^{-3}	2.00	4.71×10^{-3}	2.00	8.30×10^{-3}	1.95
2^{-7}	1.11×10^{-3}	2.02	1.16×10^{-3}	2.02	2.07×10^{-3}	2.00
2^{-8}	2.58×10^{-4}	2.10	2.70×10^{-4}	2.10	4.99×10^{-4}	2.05

detected, which validates the asymptotic compatibility property of the proposed spatial discretization scheme.

Example 4.3. We use this example to investigate nonlocal wave propagation in multi-scale media. The initial values are respectively set as

$$q(x,0)=e^{-2(x-3)^2}, \quad q_t(x,0)=0; \tag{4.4}$$

$$q(x,0)=e^{-2(x+3)^2}+e^{-2(x-3)^2}, \quad q_t(x,0)=0; \tag{4.5}$$

$$q(x,0)=e^{-4(x-10)^2}, \quad q_t(x,0)=-8(x-10)e^{-4(x-10)^2}. \tag{4.6}$$

The spatially inhomogeneous kernel (2.6) is set with the following parameter functions

$$\zeta(\beta)=\mathrm{erfc}(\beta/10), \quad \sigma(\beta)=1. \tag{4.7}$$

See Fig. 4 for the illustrations. This kind of kernel function models a nonlocal medium (negative real axis) and a "purely" local medium (positive real axis) which are glued together via heterogeneous localization [28] in a smooth manner. That is to say, we consider a wave propagation problem with a continuum of scales.

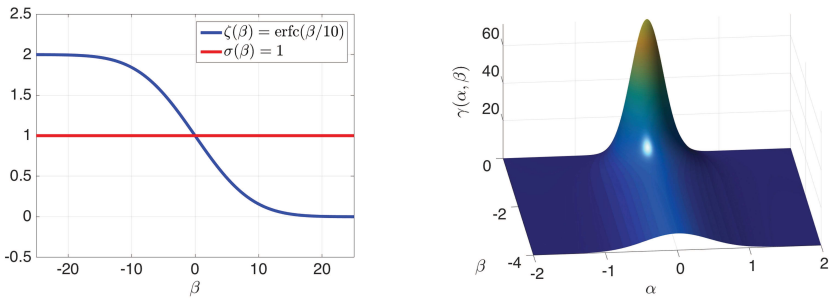

Figure 4: Kernel setting for Example 4.3. Left: plots of $\zeta(\beta)$ and $\sigma(\beta)$. Right: associated kernel function $\gamma(\alpha,\beta)$.

Since the above problem contains a continuum of scales with the small scales approaching zero, it is not clear how to analytically compute a reliable reference solution, even with sufficiently refined spatial meshes and time steps. From the design point of view, an asymptotically compatible numerical scheme is a good candidate for handling such kind of problems [28]. For this example, we employ our asymptotically compatible finite difference method to compute the numerical solutions.

The computational parameters are set as $h=2^{-7}$, $\tau=5\times10^{-3}$, and $\kappa=50$. Fig. 5 illustrates the numerical solutions with the single Gaussian initial value (4.4) up to $T=20$ over the computational domain $[-20,25]$. We observe different wave propagation behaviors when two split waves travel into the left nonlocal medium and the right "local" medium. While the wave in the local medium maintains its package form, the wave in

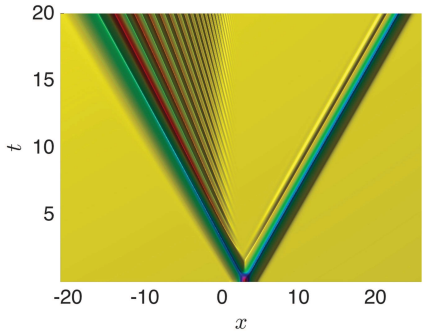

Figure 5: Numerical solution of Example 4.3 up to $T=20$ with the initial values (4.4). The left nonlocal region is connected with the right "local" region in a smooth manner.

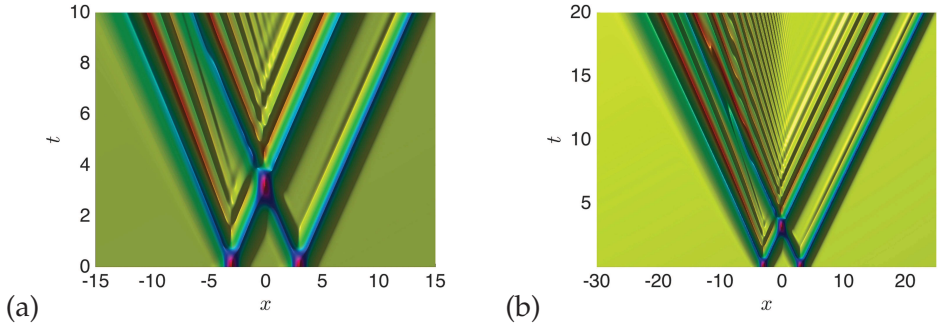

Figure 6: Numerical solution of Example 4.3 with the initial values (4.5). (a) $T=10$ and the computational domain $[-15,15]$; (b) $T=20$ and the computational domain $[-30,25]$. The left nonlocal region is connected with the right "local" region in a smooth manner.

the nonlocal medium is slightly slowed down and split into a sequence of small wave packets.

Fig. 6 illustrates the numerical solutions with the double Gaussian initial value (4.5) up to $T=10$ and $T=20$ over the computational domain $[-15,15]$ and $[-20,25]$, respectively. Again, one can see that different wave propagation behaviors when four split waves travel into the left nonlocal medium and the right "local" medium. While the wave in the local medium maintains its package form, and the wave in the nonlocal medium is slightly slowed down and collides each other and splits into a sequence of small wave packets.

The panel (a) in Fig. 7 illustrates the numerical solutions with the initial value (4.6) up to $T=15$ over the computational domain $[-10,25]$. The panel (b) in Fig. 7 illustrates the difference between numerical solutions of multi-scale medium problems and numerical solutions of the classical local wave equation. This kind of initial values make the single-directional wave propagation travel from the right "local" medium to the left "nonlocal" medium. Again, while the wave in the local medium maintains its package form, and the

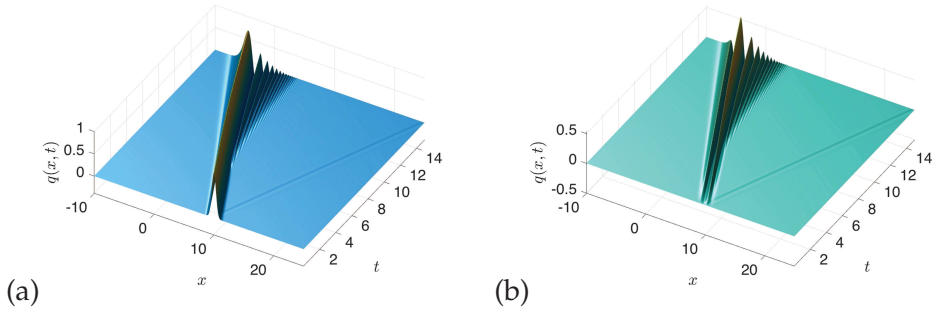

Figure 7: (a) Numerical solution of Example 4.3 with the initial values (4.6) over $T=15$ and the computational domain $[-10,25]$; (b) The difference between numerical solutions of multi-scale medium problems and numerical solutions of the classical local wave equation with the initial value (4.6) up to $T=15$. The left nonlocal region is connected with the right "local" region in a smooth manner.

wave in the nonlocal medium is slightly slowed down and becomes a sequence of small wave packets with different velocities.

To verify the reliability of the numerical solutions, we perform the following numerical tests. While maintaining the time step sufficiently small, we successively refine the spatial mesh sizes by two to examine the numerical convergence orders with initial values (4.4), (4.5) and (4.6). In Table 5, we list the L^2-errors between two successive numerical solutions and the associated convergence orders. A second order can be detected, which implies the effectiveness of our asymptotically compatible scheme.

Table 5: (Example 4.3) L^2-errors and convergence orders by reducing h at finial time $T=10$.

With initial value (4.4): h	2^{-4}	2^{-5}	2^{-6}	2^{-7}
L^2-errors over domain $[-16,20]$	4.51×10^{-3}	1.09×10^{-3}	2.71×10^{-4}	6.78×10^{-5}
order	–	2.06	2.00	2.00
With initial value (4.5): h	2^{-4}	2^{-5}	2^{-6}	2^{-7}
L^2-errors over domain $[-16,20]$	6.41×10^{-3}	1.38×10^{-3}	3.05×10^{-4}	7.01×10^{-5}
order	–	2.18	2.12	2.12
With initial value (4.6): h	2^{-4}	2^{-5}	2^{-6}	2^{-7}
L^2-errors over domain $[-3,20]$	3.36×10^{-3}	7.79×10^{-4}	1.95×10^{-4}	4.87×10^{-5}
order	–	2.11	2.00	2.00

5 Discussion

The aim of this paper is to simulate the nonlocal wave-propagation in multi-scale mediums by employing AC scheme and constructing efficient ABCs. The introduction of AC scheme makes numerical solutions reliable as $\delta\to0$, and the introduction of ABCs is used

to reformulate the infinite ODE system to a finite ODE system. As what one can see in the numerical examples above, the nonlocal wave propagation is different from the local wave propagation. We take the parameter functions $\sigma(\beta)=1$, $\zeta(\beta)=\delta$ for example to understand the nonlocal wave propagation behaviors for various δ. In this situation, the well-documented dispersion relations, see [6] for example, is given as

$$\omega^2=\int(1-e^{ik\alpha})\gamma(\alpha,\beta)d\alpha=\frac{40}{\delta^2}\left(1-e^{-\frac{\delta^2k^2}{40}}\right), \tag{5.1}$$

where we use the fact in this example that

$$\gamma(\alpha,\beta)=\frac{\sigma(\beta)}{\zeta^3(\beta)}H\left(\frac{\alpha}{\zeta(\beta)}\right)=\frac{4\sqrt{10^3/\pi}}{\delta^3}e^{-\frac{10\alpha^2}{\delta^2}}.$$

As $\delta\to 0$, we recover the dispersive relation $\omega^2=k^2$ for the local wave equation. The group velocity v_g and phase velocity v_p are defined by the equations:

$$v_g=\frac{\partial\omega}{\partial k}=\frac{ke^{-\frac{\delta^2k^2}{40}}}{\sqrt{\frac{40}{\delta^2}(1-e^{-\frac{\delta^2k^2}{40}})}};\quad v_p=\frac{\omega}{k}=\frac{\sqrt{40}}{k\delta}\sqrt{1-e^{-\frac{\delta^2k^2}{40}}}.$$

By using the first order Taylor expansion, it is easy to see that

$$v_g\approx e^{-\frac{\delta^2k^2}{40}};\qquad v_p\approx 1.$$

Again, one can see that $v_g=v_p=1$ as $\delta\to 0$ for the classical local wave equation, which implies that a wave of any shape will travel undistorted at this velocity. For the nonlocal wave equation, ω is not a linear function of k, the envelope of a wave package does not move at a single velocity, but its wavenumber components (k) move at different velocities, distorting the envelope. When $\delta\to 0$, the dispersion relation (5.1) can be approximated by a linear function over a narrow range of frequencies, the pulse distortion will be small. In this sense, we can have an insightful understanding of the nonlocal wave propagation in Figs. 1 and 3 for various values of δ.

Furthermore, we use Example 4.3 to present wave propagation problems with a continuum of scales of horizon, which model a nonlocal medium (in the negative real axis) and a "purely" local medium (in the positive real axis) glued together in a smooth manner via heterogeneous localization. We refer to [28] for more mathematical studies of nonlocal models with this type of heterogeneously localized horizon. Numerical simulations show that the wave in the local media is nondispersive when traveling along the positive axis, and the wave in the nonlocal media is dispersive when traveling along the negative axis.

Appendix: Fast algorithm for second-order operator difference equation

Let $\mathfrak{H}$ be a Hilbert space. The bounded linear operators on $\mathfrak{H}$ are denoted by $\mathcal{B}(\mathfrak{H})$. Given two operators A_0 and B_0 in $\mathcal{B}(\mathfrak{H})$, we consider the following second-order operator difference equation

$$x_n = A_0 x_{n-1} + B_0 x_{n+1}. \tag{A.1}$$

We assume that for all $x_0 \in \mathfrak{H}$ and $x_{N+1} \in \mathfrak{H}$ with $N \geq 0$, Eq. (A.1) admits a unique sequence solution $\{x_n\}_{n=0}^{N+1}$.

Now let us consider the semi-infinite second-order operator difference equation

$$\begin{aligned} &x_n = A_0 x_{n-1} + B_0 x_{n+1}, \quad n \geq 1, \\ &x_n \to 0, \quad n \to \infty. \end{aligned} \tag{A.2}$$

We assume that for all $x_0 \in \mathfrak{H}$, the above problem admits a unique sequence solution $\{x_n\}_{n\geq 0}$. Under this assumption, we know that there exists a linear mapping $\mathcal{K} \in \mathcal{B}(\mathfrak{H})$, such that

$$x_1 = \mathcal{K} x_0.$$

We intend to determine the operator T in an efficient manner. Let us put

$$y_n^{(k)} = x_{2^k n}, \quad k \geq 0, \quad n \geq 0.$$

Then we have $y_0^{(k)} = x_0$ for all $k \geq 0$. Note that the equation (A.2) can be rewritten as

$$\begin{aligned} &y_n^{(0)} = A_0 y_{n-1}^{(0)} + B_0 y_{n+1}^{(0)}, \quad n \geq 1, \\ &y_0^{(0)} = x_0, \\ &y_n^{(0)} \to 0, \quad n \to \infty. \end{aligned}$$

In particular we have

$$x_1 = y_1^{(0)} = A_0 y_0^{(0)} + B_0 y_1^{(1)} = A_0 x_0 + B_0 y_1^{(1)}. \tag{A.3}$$

Since

$$\begin{pmatrix} -A_0 & I & -B_0 & & \\ & -A_0 & I & -B_0 & \\ & & -A_0 & I & -B_0 \end{pmatrix} \begin{pmatrix} y_{n-2}^{(0)} \\ y_{n-1}^{(0)} \\ y_n^{(0)} \\ y_{n+1}^{(0)} \\ y_{n+2}^{(0)} \end{pmatrix} = 0, \quad n \geq 2,$$

we derive

$$y_n^{(0)} = A_1 y_{n-2}^{(0)} + B_1 y_{n+2}^{(0)}, \quad n \geq 2, \tag{A.4}$$

where

$$\begin{pmatrix} A_1 & B_1 \end{pmatrix} = \begin{pmatrix} 0 & I & 0 \end{pmatrix} \begin{pmatrix} I & -B_0 & 0 \\ -A_0 & I & -B_0 \\ 0 & -A_0 & I \end{pmatrix}^{-1} \begin{pmatrix} A_0 & 0 \\ 0 & 0 \\ 0 & B_0 \end{pmatrix}.$$

In particular, Eq. (A.4) arrives at

$$\begin{aligned} &y_n^{(1)} = A_1 y_{n-1}^{(1)} + B_1 y_{n+1}^{(1)}, \quad n \geq 1, \\ &y_0^{(1)} = x_0, \\ &y_n^{(1)} \to 0, \quad n \to \infty, \end{aligned}$$

which leads to

$$y_1^{(1)} = A_1 y_0^{(1)} + B_1 y_1^{(2)} = A_1 x_0 + B_1 y_1^{(2)}.$$

Recursively, for all $m \geq 1$, we have

$$\begin{aligned} &y_n^{(m)} = A_m y_{n-1}^{(m)} + B_m y_{n+1}^{(m)}, \quad n \geq 1, \\ &y_0^{(m)} = x_0, \\ &y_n^{(m)} \to 0, \quad n \to \infty, \end{aligned}$$

where

$$\begin{pmatrix} A_m & B_m \end{pmatrix} = \begin{pmatrix} 0 & I & 0 \end{pmatrix} \begin{pmatrix} I & -B_{m-1} & 0 \\ -A_{m-1} & I & -B_{m-1} \\ 0 & -A_{m-1} & I \end{pmatrix}^{-1} \begin{pmatrix} A_{m-1} & 0 \\ 0 & 0 \\ 0 & B_{m-1} \end{pmatrix}. \tag{A.5}$$

Besides, for all $m \geq 1$, it holds that

$$y_1^{(m)} = A_m y_0^{(m)} + B_m y_1^{(m+1)} = A_m x_0 + B_m y_1^{(m+1)}.$$

Recalling (A.3) and the above, we derive

$$x_1 = \{A_0 + B_0[A_1 + B_1[\cdots + B_{m-1}[A_m + B_m[\cdots]]]]\} x_0,$$

which implies that

$$\mathcal{K} = A_0 + B_0[A_1 + B_1[\cdots + B_{m-1}[A_m + B_m[\cdots]]]]. \tag{A.6}$$

By truncating the series terms in the above formula, we arrive at an approximation of the operator $\mathcal{K}$. The truncation criterion is to introduce a tolerance error, set to be $\epsilon := 10^{-14}$ here, such that the L^2-norms of A_m and B_m in (A.5) are less than the given tolerance ϵ. This leads to an efficient way of evaluating $\mathcal{K}$ in (A.6) for the problem considered in this paper. It turns out that the maximum number of the iteration to obtain the converged $\mathcal{K}$ for the given ϵ is less than 20 in all the simulations above.

Acknowledgments

Qiang Du is supported in part by the U.S. NSF grants DMS-1719699, AFOSR MURI Center for material failure prediction through peridynamics, and the ARO MURI W911NF-15-1-0562 on Fractional PDEs for Conservation Laws and Beyond: Theory, Numerics and Applications. Jiwei Zhang is partially supported by NSFC under grant Nos. 11771035, 91430216 and U1530401. Chunxiong Zheng is partially supported by NSFC under grant Nos. 11771248, 91630205, 11371218. The authors are grateful to the fruitful discussions with Prof. Houde Han.

References

[1] B. Alpert, L. Greengard, and T. Hagstrom, *Rapid evaluation of nonreflecting boundary kernels for time-domain wave propagation*, SIAM J. Numer. Anal., 37 (2000), 1138-1164.
[2] A. Arnold, M. Ehrhardt, and I. Sofronov, *Approximation, stability and fast calculation of nonlocal boundary conditions for the Schrödinger equation*, Commun. Math. Sci., 1 (2003), 501-556.
[3] F. Bobaru, M. Yang, L.F. Alves, S.A. Silling, E. Askari, J. Xu, Convergence, adaptive refinement, and scaling in 1D peridynamics, Internat. J. Numer. Methods Engrg. 77 (2009), 852-877.
[4] F. Bobaru and M. Duangpanya, *The peridynamic formulation for transient heat conduction*, Internat. J. of Heat and Mass Transfer, 53(2010), 4047-4059.
[5] Q. Du, *From peridynamics to stochastic jump process: Illustrations of nonlocal balance laws and nonlocal calculus framework*, Scientia Sinica, 45 (7) (2015), 939-952.
[6] Q. Du, *Local limits and asymptotically compatible discretizations*, in Handbook of peridynamic modeling, Adv. Appl. Math., CRC Press, Boca Raton, FL, 2017, 87-108.
[7] Q. Du, M. Gunzburger, R.B. Lehoucq and K. Zhou, *A nonlocal vector calculus, nonlocal volume-constrained problems, and nonlocal balance laws*, Math. Mod. Meth. Appl. Sci., 23(2013), 493-540.
[8] Q. Du, M. Gunzburger, R. Lehoucq and K. Zhou, *Analysis and approximation of nonlocal diffusion problems with volume constraints*, SIAM Rev., 54(2012), 667-696.
[9] Q. Du, Y. Tao, X. Tian and J. Yang, *Asymptotically compatible discretization of multidimensional nonlocal diffusion models and nonlocal gradient recovery*. Submitted, 2017.
[10] Q. Du, J. Zhang and C. Zheng, *Numerical solution of a two-dimensional nonlocal wave equation on unbounded domains.* To appear in SIAM J. Sci. Comput., 2018.
[11] D. Givoli, High-order local non-reflecting boundary conditions: A review, Wave Motion, 39 (2004), pp. 319-326.
[12] I. S. Gradshteyn and I. M. Ryzhik, Tables of Integrals, Series, and Products, 6th ed. San Diego, CA: Academic Press, page 1090, 2000.
[13] M. J. Grote and J. B. Keller, *Exact nonreflecting boundary conditions for the time dependent wave equation*, SIAM J. Appl. Math., 55 (1995), 280-297.
[14] T. Hagstrom, *New results on absorbing layers and radiation boundary conditions, in Topics in Computational Wave Propagation,* M. Ainsworth et al., eds., Springer-Verlag, New York, 2003, 1-42.
[15] T. Hagstrom, A. Mar-Or, D. Givoli, *High-order local absorbing conditions for the wave equation: Extensions and improvements*, J. Comput. Phys., 227 (2008), 3322-3357.
[16] H. Han and Z. Huang, *A class of artificial boundary conditions for heat equation in unbounded domains,* Comput. Math. Appl., 43(2002), 889-900.

[17] H. Han and X. Wu, *Artificial boundary method*, Spring-Verlag and Tsinghua Unversity Press, Berlin Heidelberg and Beijing, 2013.
[18] H. Han and C. Zheng, *Exact nonreflecting boundary conditions for an acoustic problem in three dimensions*, J. Comput. Math., 21 (2003), 15-24.
[19] S. G. Krantz, Handbook of Complex Variables. Boston, MA: Birkhäuser, page 93, 1999.
[20] G. Pang, Y. Yang, and S. Tang, *Exact boundary condition for semidiscretized Schrödinger equation and heat equation in a rectangular domain,* J. Sci. Comp., 72 (2017), 1-13.
[21] M. Rizzardi, *A modification of Talbot's method for the simultaneous approximation of several values of the inverse Laplace transform*, ACM Trans. Math. Software, 21 (1995), 347-371.
[22] S. Silling, *Reformulation of elasticity theory for discontinuities and long–range forces*, J. Mech. Phys. Solids, 48 (2000), 175-209.
[23] S. Silling, E. Askari, A gridfree method based on the peridynamic model of solid mechanics, Comput. Struct. 83 (2005), 1526-1535.
[24] A. Talbot, *The accurate numerical inversion of Laplace transforms*, J. Inst. Math. Appl., 23 (1979), 97-120.
[25] H. Tian, L. Ju and Q. Du, *A conservative nonlocal convection-diffusion model and asymptotically compatible finite difference discretization*, Comput. Methods Appl. Mech. Engrg., 320 (2017), 46-67.
[26] X. Tian and Q. Du, *Analysis and comparison of different approximations to nonlocal diffusion and linear peridynamic equations*, SIAM J. Numer. Anal., 51(2013), 3458-3482.
[27] X. Tian and Q. Du, *Asymptotically compatible schemes and applications to robust discretization of nonlocal models*, SIAM J. Numer. Anal., 52 (2014), 1641-1665.
[28] X. Tian and Q. Du, *Trace theorems for some nonlocal function spaces with heterogeneous localization*, SIAM J. Math. Anal., 49 (2017), 1621-1644.
[29] Z. H. Teng, *Exact boundary condition for time-dependent wave equation based on boundary integral*, J. Comput. Phys., 190 (2003), 398-418.
[30] L. Ting and M. J. Miksis, *Exact boundary conditions for scattering problems*, J. Acoust. Soc. Amer., 80 (1986), 1825-1827.
[31] S. V. Tsynkov, *Numerical solution of problems on unbounded domains: A review*, Appl. Numer. Math., 27 (1998), 465-532.
[32] L. Verlet, *Computer Experiments on Classical Fluids. I. Thermodynamical Properties of Lennard-Jones Molecules*, Phys. Rev. 159 (1967), 98–103.
[33] X. Wang and S. Tang, *Matching boundary conditions for lattice dynamics*, Int J. Numer Meth. Eng., 93(12) (2013),1255-1285.
[34] O. Weckner, R. Abeyaratne, *The effect of long-range forces on the dynamics of a bar,* J. Mech. Phys. Solids 53 (2005), 705-728.
[35] J.A.C. Weideman, *Optimizing Talbots contours for the inversion of the Laplace transform,* SIAM J. Numer. Anal., 44(6) (2006), 2342-2362.
[36] R.A. Wildman and G.A. Gazonas, *A perfectly matched layer for peridynamics in two dimensions*, J. Mech. Mater. Struct., 7:8-9 (2012), 765-781.
[37] W. Zhang, J. Yang, J. Zhang and Q. Du, *Absorbing boundary conditions for nonlocal heat equations on unbounded domain*, Commun. Comput. Phys., 21 (2017), 16-39.
[38] C. Zheng, J. Hu, J. Zhang and Q. Du, *Numerical solution of the nonlocal diffusion equation on the real line*, SIAM J. Sci. Comput., 39(5) (2017), A1951-A1968.
[39] K. Zhou and Q. Du, *Mathematical and Numerical Analysis of Linear Peridynamic Models with Nonlocal Boundary Conditions*, SIAM J. Numer. Anal., 48 (2010), 1759-1780.